The Astrophysical Journal, 650:604–613, 2006 October 20

CO(1–0) IN $z \gtrsim 4$ QUASAR HOST GALAXIES: NO EVIDENCE FOR EXTENDED MOLECULAR GAS RESERVOIRS

Dominik A. Riechers,[1] Fabian Walter,[1] Christopher L. Carilli,[2] Kirsten K. Knudsen,[1] K. Y. Lo,[3] Dominic J. Benford,[4] Johannes G. Staguhn,[4] Todd R. Hunter,[5] Frank Bertoldi,[6] Christian Henkel,[7] Karl M. Menten,[7] Axel Weiss,[7] Min S. Yun,[8] and Nick Z. Scoville[9]

Received 2005 October 26; accepted 2006 June 16

ABSTRACT

We present ^{12}CO($J = 1 \rightarrow 0$) observations of the high-redshift quasi-stellar objects (QSOs) BR 1202−0725 ($z = 4.69$), PSS J2322+1944 ($z = 4.12$), and APM 08279+5255 ($z = 3.91$) using the NRAO Green Bank Telescope (GBT) and the MPIfR Effelsberg 100 m telescope. We detect, for the first time, the CO ground-level transition in BR 1202−0725. For PSS J2322+1944 and APM 08279+5255, our observations result in line fluxes that are consistent with previous NRAO Very Large Array (VLA) observations, but they reveal the full line profiles. We report a typical lensing-corrected velocity-integrated intrinsic ^{12}CO($J = 1 \rightarrow 0$) line luminosity of $L'_{\rm CO} = 5 \times 10^{10}$ K km s^{-1} pc^2 and a typical total H_2 mass of $M(H_2) = 4 \times 10^{10}\ M_\odot$ for the sources in our sample. The CO/FIR luminosity ratios of these high-z sources follow the same trend as seen for low-z galaxies, leading to a combined solution of $\log L_{\rm FIR} = (1.39 \pm 0.05) \log L_{\rm CO} - 1.76$. It has previously been suggested that the molecular gas reservoirs in some quasar host galaxies may exhibit luminous, extended ^{12}CO($J = 1 \rightarrow 0$) components that are not observed in the higher J CO transitions. Using the line profiles and the total intensities of our observations and large velocity gradient (LVG) models based on previous results for higher J CO transitions, we derive that emission from all CO transitions is described well by a single gas component in which all molecular gas is concentrated in a compact nuclear region. Thus, our observations and models show no indication of a luminous extended, low surface brightness molecular gas component in any of the high-redshift QSOs in our sample. If such extended components exist, their contribution to the overall luminosity is limited to at most 30%.

Subject headings: cosmology: observations — galaxies: active — galaxies: formation — galaxies: high-redshift — galaxies: ISM — galaxies: starburst

Online material: color figures

1. INTRODUCTION

Understanding when and how galaxies form is one of the primary objectives in both observational and theoretical astrophysics. The mere fact that active galaxies, such as radio galaxies, quasi-stellar-objects (QSOs), and emission-line galaxies are observed up to redshifts of $z = 6.6$ (e.g., Fan et al. 2001; Rhoads & Malhotra 2001; Hu et al. 2002; Kodaira et al. 2003; Taniguchi et al. 2005), less than 1 Gyr after recombination, implies that galactic-scale (∼10 kpc), gravitationally bound structures exist at this early epoch. The study of the masses and dynamical state of these young systems serves as a direct constraint to the models describing the growth of large-scale structures since the epoch of recombination.

Studies of the molecular and dusty interstellar medium (ISM) in these galaxies are of fundamental importance, since it is this medium out of which stars form; accurate determination of the molecular gas mass could therefore serve as an indicator of the evolutionary state of a galaxy. The detection of carbon monoxide (CO) is also a strong confirmation that star formation is going on in some of the highest redshift systems. In fact, the combination of molecular gas and dust detections with large far-infrared (FIR) luminosities provides the strongest evidence that a significant fraction of high-z galaxies are undergoing starbursts at prodigious rates ($>10^3\ M_\odot$ yr^{-1}), consistent with the formation of a large elliptical galaxy on a dynamical timescale of $\sim 10^7$–10^8 yr.

Over the past decade, more than 30 galaxies at $z > 2$ have been detected in CO emission (Solomon & Vanden Bout 2005) out to a redshift of $z = 6.42$ (Walter et al. 2003, 2004; Bertoldi et al. 2003), confirming the presence of intense starbursts in numerous high-z galaxies. As most of these observations were obtained using millimeter interferometers, these detections were typically achieved by observing high-J CO($J \rightarrow J - 1$) transitions ($J \geq 3$). Although these high-J lines exhibit in general higher peak flux densities than the ground-state ($J = 1$) transition, it is possible that the higher order transitions are biased to the excited gas close to a central starburst and do not necessarily trace the entire molecular gas reservoir seen in ^{12}CO($J = 1 \rightarrow 0$). In addition, the conversion factor (α) to derive molecular (H_2) masses from measured CO luminosities has mostly been estimated for the ^{12}CO($J = 1 \rightarrow 0$) line (e.g., Downes & Solomon 1998; Weiss et al. 2001). Observing ^{12}CO($J = 1 \rightarrow 0$) has the additional advantage that properties of the highly redshifted sources

[1] Max-Planck-Institut für Astronomie, Königstuhl 17, Heidelberg, D-69117, Germany.
[2] National Radio Astronomy Observatory, P.O. Box O, Socorro, NM 87801.
[3] National Radio Astronomy Observatory, 520 Edgemont Road, Charlottesville, VA 22903-2475.
[4] Laboratory for Observational Cosmology, Code 665, NASA Goddard Space Flight Center, Greenbelt, MD 20771.
[5] Harvard-Smithsonian Center for Astrophysics, 60 Garden Street, Cambridge, MA 01238.
[6] Radioastronomisches Institut, Universität Bonn, Auf dem Hügel 71, Bonn, D-53121, Germany.
[7] Max-Planck-Institut für Radioastronomie, Auf dem Hügel 69, Bonn, D-53121, Germany.
[8] Department of Astronomy, University of Massachusetts, 710 North Pleasant Street, Amherst, MA 01003.
[9] Astronomy Department, California Institute of Technology, Mail Code 105-24, 1200 East California Boulevard, Pasadena, CA 91125.

can be *directly* compared to the molecular gas properties of nearby (starburst) galaxies that are predominantly mapped in the ^{12}CO($J = 1 \rightarrow 0$) transition.

These are main motivations for observing the ^{12}CO($J = 1 \rightarrow 0$) ground-state transition. However, due to the faintness of the line and the bandwidth limitations of current radio telescopes, such high-z ^{12}CO($J = 1 \rightarrow 0$) observations only exist for two QSOs and two radio galaxies to date. All of these observations have been obtained with radio interferometers operating at centimeter wavelengths: the NRAO Very Large Array (VLA; Papadopoulos et al. 2001; Carilli et al. 2002a; Greve et al. 2004) and the Australia Telescope Compact Array (ATCA; Klamer et al. 2005). In particular, due to the bandwidth limitations of the VLA, obtaining better constraints on the spectral line shape and total flux of the ^{12}CO($J = 1 \rightarrow 0$) transition is desirable even for already detected sources. Today's largest single-dish telescopes, such as the NRAO Green Bank Telescope (GBT)[10] and the MPIfR Effelsberg telescope,[11] can eliminate some of those issues due to their larger spectral bandwidths.

Here we report on first observations of ^{12}CO($J = 1 \rightarrow 0$) in three CO-bright high-z QSOs, which also exhibit ultraluminous IR emission, using the GBT and the Effelsberg telescope. In § 2, we describe our observations. Section 3 summarizes our results on the individual objects (BR 1202−0725 at $z = 4.69$, PSS J2322+1944 at $z = 4.12$, and APM 08279+5255 at $z = 3.91$). Section 4 provides an analysis and discussion, and § 5 closes with a summary of our results. We assume a standard ΛCDM cosmology throughout, with $H_0 = 71$ km s^{-1} Mpc^{-1}, $\Omega_M = 0.27$, and $\Omega_\Lambda = 0.73$ (Spergel et al. 2003).

2. OBSERVATIONS

2.1. *Green Bank Telescope*

Observations of the three targets were carried out with the GBT during 12 observing runs between 2004 October and 2005 April with a total observing time of 89.5 hr. The total/on-source observing times were 31.5/20 hr for BR 1202−0725, 23/15 hr for PSS J2322+1944, and 35/22 hr for APM 08279+5255. During all runs, 3C 147 and 3C 286 were used as primary/flux calibrators. For spectral line calibration, we observed IRC +10216, DR 21, Orion IRc2, Orion HC, and W3OH H_2O. As secondary/pointing calibrators, 3C 273, J1256−0547 (for BR 1202−0725), J2253+1608 (for PSS J2322+1944), J0753+538, and J0824+5552 (for APM 08279+5255) were used. The pointing accuracy, determined by continuum cross scans of nearby sources, was typically $\sim 3''$ (reaching $\lesssim 1''$ under the best conditions). We estimate the calibration to be accurate to 10%–15%. As the ^{12}CO($J = 1 \rightarrow 0$) transition at 115.2712 GHz is redshifted into the K band for all three targets (BR 1202−0725: $\nu_{\rm obs} = 20.2450$ GHz; PSS J2322+1944: $\nu_{\rm obs} = 22.5258$ GHz; APM 08279+5255: $\nu_{\rm obs} = 23.4663$ GHz), the dual-beam, dual-polarization 18–26 GHz receiver was used for all observations. The beam size of the GBT at our observing frequencies is $\sim 32''$–$36''$ ($\sim$225–250 kpc at $z \simeq 4$), i.e., much larger than our targets. The two beams have a fixed separation of $178''.8$ in the azimuth direction. Two different spectrometer setups were used; half of the observing runs were executed in the first mode, and the other half of the runs in the second mode. The first mode features two simultaneous intermediate frequencies (IFs) with a bandwidth of 800 MHz ($\sim$10,000–12,000 km s^{-1} at our observing frequencies) and 2048 channels each, resulting in a spectral resolution of 391 kHz ($\sim$5 km s^{-1}). The ^{12}CO($J = 1 \rightarrow 0$) line was always centered in the first 800 MHz IF. The second mode has one IF with 200 MHz ($\sim$2500–3000 km s^{-1}) and 16,384 channels, resulting in a spectral resolution of 12 kHz ($\sim$0.15 km s^{-1}). BR 1202−0725 and APM 08279+5255 were observed with both setups, while PSS J2322+1944 was only observed during runs that used the second setup. The spectra taken in each mode were examined separately and then combined. The ON-OFF position switching mode was used; i.e., the target was observed alternately with the two telescope beams, and the off-source beam was always monitoring the sky background in parallel. The beam switching frequency was once every 60–120 s depending on the observing run. The weather was excellent for the winter nights with typical zenith system temperatures of $T_{\rm sys} = 22$–35 K on a $T_A^\star$ scale. On 2005 April 19 and 20 the system temperatures were significantly higher (typically $T_{\rm sys} = 50$–60 K).

For data reduction, the AIPS++[12] package and the new GBT IDL software[13] were used, providing consistent results. The spectra of BR 1202−0725, PSS J2322+1944, and APM 08279+5255 were binned to 2.00 MHz (30 km s^{-1}), 1.80 MHz (24 km s^{-1}), and 5.86 MHz (75 km s^{-1}), reaching rms noise values of $\sim$75, $\sim$140, and $\sim$65 μJy, respectively. A linear baseline was subtracted from the PSS J2322+1944 spectrum to remove continuum fluxes and atmospheric/instrumental effects. For BR 1202−0725 and APM 08279+5255, polynomials of order 2 have been used to remove a very wide ($\gg$100 MHz, i.e., much broader than the width of the CO line) "bending" of the baselines. Only the frequency range that was used to define the spectral baselines is used for the final GBT spectra. APM 08279+5255 was observed using both the 200 and 800 MHz bandwidth setups. While the ^{12}CO($J = 1 \rightarrow 0$) line was clearly detected with both setups, the spectrum obtained with the narrowband high-resolution 200 MHz setup shows significant baseline problems, as the continuum level is significantly different on the red and blue sides of the line. Therefore, we only use the results obtained with the wide 800 MHz bandwidth setup (corresponding to 15 hr on-source, and covering a velocity range of $\sim$8000 km s^{-1}) for the final spectrum. In addition to simple ON-OFF combinations and subtraction of low-order polynomial spectral baselines, we also followed the scheme proposed by Vanden Bout et al. (2004) for reconstructing the temporal baseline variations; however, we found that this did not improve our final results. The reduced spectra were read into GILDAS/CLASS[14] to write out the final combined spectrum tables. The final spectra are shown in the top panels of Figures 1 and 2 and in Figure 3. We note that the spectrum of BR 1202−0725 is limited to the central $\sim$150 MHz due to the fact that about half of the data were taken with the narrower 200 MHz setting.

2.2. *Effelsberg Telescope*

Observations were carried out toward BR 1202−0725 and PSS J2322+1944 in 2003 January and February with a total observing time of $\sim$40 hr (20 hr per source, corresponding to 8 hr on-source each). At $40''$ beam size, the pointing accuracy, as determined by continuum cross scans of nearby sources, was better than $10''$, with typical values of $\sim 5''$. Calibrations for the gain as well as the variation of the atmospheric opacity and zenith distance were obtained from observations of 3C 286 and NGC 7027 (see Ott et al. 1994 for reference fluxes), leading to a

[10] The Green Bank Telescope is a facility of the National Radio Astronomy Observatory (NRAO), operated by Associated Universities, Inc., under a cooperative agreement with the National Science Foundation.

[11] The Effelsberg telescope is a facility of the Max-Planck-Gesellschaft (MPG), operated by the Max-Planck-Institut für Radioastronomie (MPIfR).

[12] See http://aips2.nrao.edu.

[13] See http://gbtidl.sourceforge.net.

[14] See http://www.iram.fr/IRAMFR/GILDAS/.

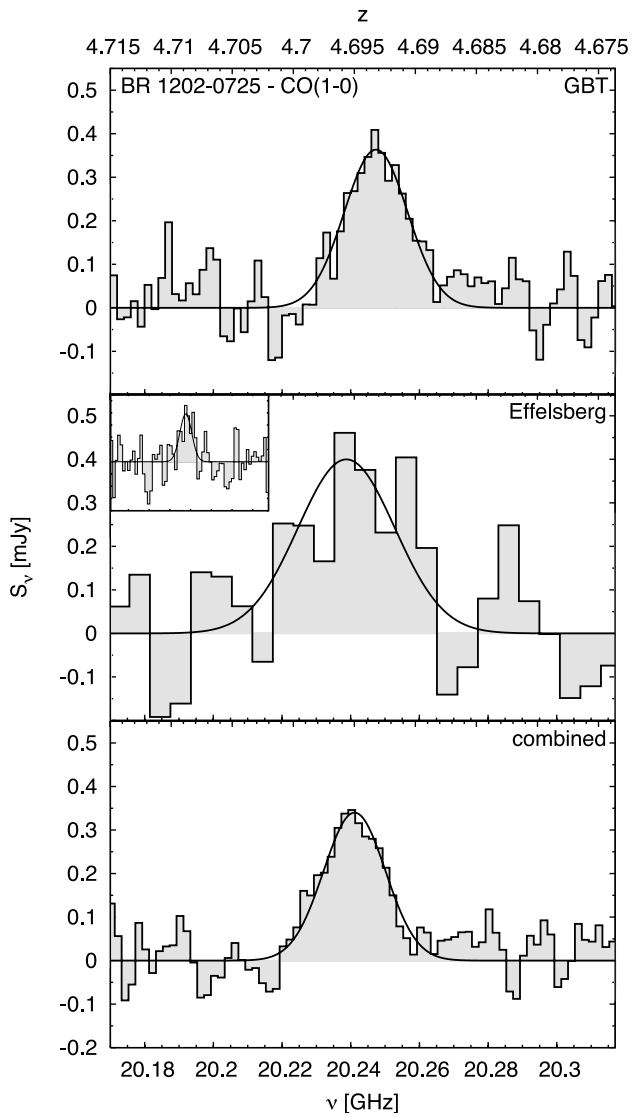

FIG. 1.—GBT (*top*) and Effelsberg (*middle*) spectra of ^{12}CO($J = 1 \rightarrow 0$) emission from BR 1202−0725. The bottom panel shows the combined spectrum. The GBT spectrum has been smoothed to a resolution of 2.00 MHz (30 km s^{-1}). The rms per channel is ∼75 μJy. The Effelsberg spectrum has been smoothed to a resolution of 5.97 MHz (88 km s^{-1}). The rms per channel is ∼155 μJy. For illustration, the inset shows the full spectral range of the Effelsberg spectrum that was used for spectral baseline fitting (width ∼380 MHz). The combined spectrum has been smoothed to a resolution of 2.00 MHz (30 km s^{-1}). The rms per channel is ∼70 μJy. The thin black lines show Gaussian fits to the data (see Table 1). [*See the electronic edition of the Journal for a color version of this figure*.]

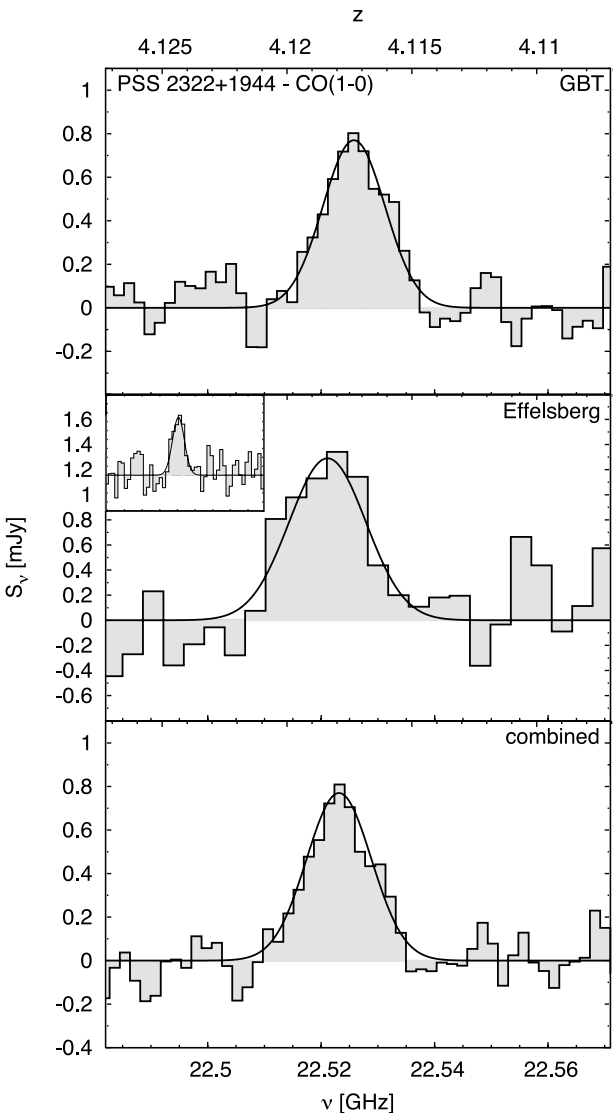

FIG. 2.—GBT (*top*) and Effelsberg (*middle*) spectra of ^{12}CO($J = 1 \rightarrow 0$) emission from PSS J2322+1944. The bottom panel shows the combined spectrum. The GBT spectrum has been smoothed to a resolution of 1.80 MHz (24 km s^{-1}). The rms per channel is ∼140 μJy. The Effelsberg spectrum has been smoothed to a resolution of 3.60 MHz (48 km s^{-1}). The rms per channel is ∼380 μJy. For illustration, the inset shows the full spectral range of the Effelsberg spectrum that was used for spectral baseline fitting (width ∼180 MHz). The combined spectrum has been smoothed to a resolution of 1.80 MHz (24 km s^{-1}). The rms per channel is ∼125 μJy. The thin black lines show Gaussian fits to the data (see Table 1). [*See the electronic edition of the Journal for a color version of this figure*.]

total formal calibration uncertainty of ∼15%. We observed in beam switching mode using a rotating horn with a beam throw of 2′ and a switching frequency of ∼1 Hz. We have used a dual polarization HEMT receiver for all observations. The autocorrelator backend was split into eight bands of 160 MHz bandwidth and 128 channels each that could individually be shifted in frequency by up to ±250 MHz relative to the recessional velocity of the targets. The final spectra cover a velocity range of ∼6000 km s^{-1} with channel spacings of ∼16 km s^{-1}. We achieved single channel system temperatures of 65 and 85 K on a $T_A^\star$ scale. After combination of both orthogonal linear polarizations, this leads to $T_{\rm sys}$ of 47 and 60 K.

The GILDAS/CLASS package was used for data reduction. All spectral baselines are of good quality and only first-order polynomial baselines had to be subtracted. The final spectra of BR 1202−0725 and PSS J2322+1944 are shown in the middle panels of Figures 1 and 2. These spectra were binned to 5.97 MHz (88 km s^{-1}) and 3.60 MHz (48 km s^{-1}), reaching rms noise values of ∼150 and ∼380 μJy, respectively. We note that the latter do not show the full ranges used for spectral baseline fitting. Those ranges (∼380 MHz for BR 1202−0725 and ∼180 MHz for PSS J2322+1944) are illustrated by the insets in the same figures.

2.3. *Combined Spectra*

As BR 1202−0725 and PSS J2322+1944 were observed with both telescopes, we also created combined spectra of both results to increase the signal-to-noise ratio and average out part of the calibrational uncertainties. The GILDAS/CLASS package was

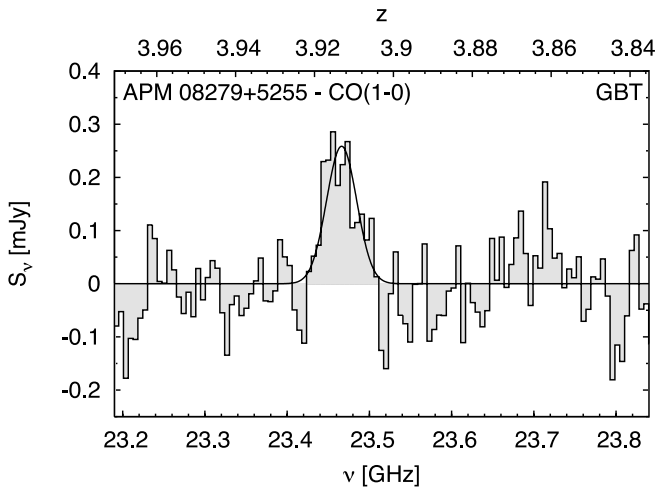

FIG. 3.—GBT spectrum of ^{12}CO($J = 1 \rightarrow 0$) emission from APM 08279+5255. The spectrum has been smoothed to a resolution of 5.86 MHz (75 km s^{-1}). The rms per channel is $\sim$65 μJy. The thin black line shows a Gaussian fit to the data (see Table 1). [*See the electronic edition of the Journal for a color version of this figure*.]

used to reprocess and combine the final spectra of both telescopes. The final unbinned GBT and Effelsberg spectra were regridded to a common velocity resolution and baseline-subtracted before combination. In the combination, spectra were weighted with their respective rms. The combined spectra of BR 1202−0725 and PSS J2322+1944, as shown in the bottom panels of Figures 1 and 2, were binned to a resolution of 2.00 MHz (30 km s^{-1}) and 1.80 MHz (24 km s^{-1}), reaching rms noise values of $\sim$70 and $\sim$125 μJy, respectively.

3. RESULTS

The sources in our study are the three CO-brightest high-redshift QSOs that can currently be observed in the ^{12}CO($J = 1 \rightarrow 0$) transition. We obtained detections for all our targets. CO line luminosities $L'_{\rm CO}$ (in K km s^{-1} pc^2) were derived using

$$L'_{\rm CO} = 3.25 \times 10^7 \left[I \nu_{\rm obs}^{-2} D_L^2 (1+z)^{-3} \right], \qquad (1)$$

where I is the velocity-integrated ^{12}CO($J = 1 \rightarrow 0$) line flux in Jy km s^{-1}, D_L is the luminosity distance in Mpc, and $\nu_{\rm obs}$ is the observed frequency in GHz (Solomon et al. 1992). For the systems with known lensing magnification factor $\mu_L^{\rm CO}$, $L'_{\rm CO}$ has to be divided by that factor in order to get the intrinsic CO luminosity of the discussed target. A conversion factor $\alpha = 0.8\, M_\odot\, {\rm K}^{-1}$ km s^{-1} pc^2 to convert $L'_{\rm CO(1-0)}$ to $M_{\rm gas}({\rm H_2})$ is assumed throughout, as applicable for local ultraluminous infrared galaxies (ULIRGs)/starbursts (Downes & Solomon 1998). All observational results are summarized in Table 1. Derived CO luminosities and gas masses as well as FIR luminosities from the literature are given in Table 2.

3.1. *BR 1202−0725*

3.1.1. *Previous Results*

BR 1202−0725 ($z = 4.69$) was detected in multiple CO transitions before (see Table 3) but not in ^{12}CO($J = 1 \rightarrow 0$). This optically bright, radio-quiet QSO has the curious property that the optical QSO is a single source, but the millimeter continuum and CO line observations show a double source with a separation of about 4″ (Omont et al. 1996; Guilloteau et al. 1999; Carilli et al. 2002b). This double morphology may indicate a pair of interacting objects separated by only 28 kpc (Yun et al. 2000; Carilli et al. 2002b). An alternative explanation would be a double-starburst system composed of a QSO (southern source) and a dust-obscured, Lyα-emitting companion (northern source; Hu et al. 1996), which is ionized by the strong QSO. Recently, Klamer et al. (2004) suggested that the nature of the double source might be due to jet-induced star formation, in which the northern component corresponds to a radio hot spot. It has been discussed that the quasar activity in this system may be triggered by gravitational interaction with the companion. Using typical conversion factors for a ULIRG (Downes & Solomon 1998), the total molecular gas mass derived from the CO luminosity exceeds the dynamical mass of the system (Carilli et al. 2002b), and as a remedy for this inconsistency, gravitational lensing has been suggested. However, the same authors argue that masses and velocity widths of the components are very different; therefore, it appears unlikely that the multiple components are different lensed images of one source.

3.1.2. *New Observations*

The final ^{12}CO($J = 1 \rightarrow 0$) spectra of BR 1202−0725 are shown in Figure 1 (*top*, GBT; *middle*, Effelsberg; *bottom*, combined spectrum). Gaussian fitting to the line profile of the combined spectrum results in a peak flux density of 0.34 ± 0.03 mJy and a FWHM of 333 ± 30 km s^{-1}. The integrated ^{12}CO($J = 1 \rightarrow 0$) line flux is 0.120 ± 0.010 Jy km s^{-1}. This agrees well

TABLE 1
OBSERVED ^{12}CO($J = 1 \rightarrow 0$) LINE PARAMETERS

Source	z	$\nu_{\rm obs}$ (GHz)	S_ν[a] (mJy)	$\Delta V_{\rm FWHM}$ (km s^{-1})	I (Jy km s^{-1})	Telescope
BR 1202−0725	4.6932 ± 0.0004	20.2450	0.36 ± 0.03	329 ± 36	0.124 ± 0.012	GBT
	4.6956 ± 0.0012	20.2388	0.40 ± 0.11	522 ± 146	0.22 ± 0.06	Effelsberg
	4.6949 ± 0.0003	20.2411	0.34 ± 0.03	333 ± 30	0.120 ± 0.010	Combined
PSS J2322+1944	4.1173 ± 0.0003	22.5258	0.77 ± 0.07	202 ± 17	0.165 ± 0.014	GBT
	4.1184 ± 0.0008	22.5211	1.29 ± 0.26	184 ± 46	0.25 ± 0.06	Effelsberg
	4.1179 ± 0.0002	22.5231	0.77 ± 0.07	190 ± 14	0.155 ± 0.013	Combined
APM 08279+5255	3.9122 ± 0.0007	23.4663	0.26 ± 0.04	556 ± 55	0.152 ± 0.020	GBT

NOTES.—All given uncertainties are formal (correlated) errors from the Gaussian fit. The z error was derived from a full three-parameter fit. In the error estimates for S_ν and $\Delta V_{\rm FWHM}$, the correlation with the error in z is neglected, as the relative uncertainty in z is $\sim$3 orders of magnitude less than that of the other two quantities. The error estimate for I takes the correlation of the errors of S_ν and $\Delta V_{\rm FWHM}$ into account.

[a] A T_A^*(K)/S(Jy) conversion factor of 1.5 was assumed for the GBT.

TABLE 2
Luminosities, Gas Masses, and Star Formation Rates

Source	D_L (Gpc)	μ_L^{CO}	L_{FIR}[a] (10^{12} $L_\odot$)	$L'_{CO(1-0)}$[a] (10^{10} K km s^{-1} pc^2)	$L_{FIR}/L'_{CO(1-0)}$ ($L_\odot$ K^{-1} km s^{-1} pc^2)	$M_{gas}(H_2)$[b] (10^{10} $M_\odot$)	SFR[c] (10^3 $M_\odot$ yr^{-1})
BR 1202−0725.....	44.2	1[d]	60[e]/60	10.1/10.1	596	8.1	9.0
PSS J2322+1944.....	37.8	2.5[f]	23[g]/9.2	10.5/4.2	219	3.4	1.4
APM 08279+5255	35.6	7[h]	200[i]/28.6	9.6/1.4	2090	1.1	4.3

[a] Apparent luminosities (not corrected for lensing)/intrinsic luminosities (lensing corrected).
[b] Assuming a conversion factor of $\alpha = 0.8\ M_\odot\ K^{-1}\ km\ s^{-1}\ pc^2$ from $L'_{CO(1-0)}$ to $M_{gas}(H_2)$ as appropriate for ULIRGs (see Downes & Solomon 1998).
[c] Assuming a Schmidt-Kennicutt law (Kennicutt 1998a, 1998b): $SFR(M_\odot\ yr^{-1}) = (1.5 \times 10^{-10}) L_{FIR}(L_\odot)$, i.e., $\delta_{MF}\delta_{SB} = 1.5$ following the notation of Omont et al. (2001), where δ_{MF} describes the dependence on the mass function of the stellar population and δ_{SB} gives the fraction of L_{FIR} that is actually powered by the starburst and not the AGN.
[d] Carilli et al. (2002b).
[e] Carilli et al. (2005).
[f] Carilli et al. (2003).
[g] Cox et al. (2002).
[h] Lewis et al. (2002).
[i] Beelen et al. (2006).

with the extrapolated value of 0.123 ± 0.013 Jy km s^{-1} derived from the ^{12}CO($J = 2 \rightarrow 1$) flux (Carilli et al. 2002b) under assumption of fully thermalized and optically thick CO emission (see also discussion in § 4.1). The width of the ^{12}CO($J = 1 \rightarrow 0$) line is consistent within the error bars with an average of the higher J transitions in the literature (∼290 km s^{-1}; see Table 3). The derived redshift of 4.6949 ± 0.0003 is in good agreement with the ^{12}CO($J = 5 \rightarrow 4$) redshift (Omont et al. 1996; northern and southern components combined). The structure of this source is unresolved at the resolution of our measurements; all line parameters are in good agreement with the higher J lines adding up both components. The derived CO line luminosity of 1.0×10^{11} K km s^{-1} pc^2 results in an H_2 gas mass of 8.1×10^{10} $M_\odot$ (see also Table 2).

TABLE 3
CO Detections in the Quasar Hosts of Our Targets in the Literature

Source	Component	z	Transition	S_ν (mJy)	I (Jy km s^{-1})	ΔV_{FWHM} (km s^{-1})	References
BR 1202-0725.....	N	4.692	2–1	0.44 ± 0.07	0.26 ± 0.05	...	1
	S	4.695	2–1	0.77 ± 0.10	0.23 ± 0.04	...	1
	NS	...	4–3	∼5.1	1.50 ± 0.3	280 ± 30	2
	N	4.6916	5–4	∼3.5	1.3 ± 0.2	350	2
	S	4.6947	5–4	∼5.5	1.1 ± 0.3	190	2
	NS	4.695	5–4	9.3 ± 2.1	2.7 ± 0.41	220 ± 74	3
	NS	4.6915	7–6	∼10.6	3.1 ± 0.86	∼275	2
PSS J2322+1944.....	...	4.1192	1–0	0.89 ± 0.22	0.19 ± 0.08	200 ± 70	4
	...	4.1192	2–1	2.70 ± 0.24	0.92 ± 0.30	280 ± 42	4, 5
	...	4.1199	4–3	10.5	4.21 ± 0.40	375 ± 41	6
	...	4.1199	5–4	12	3.74 ± 0.56	273 ± 50	6
	...	...	6–5	...	...	...	7
	...	...	7–6	...	...	...	7
APM 08279+5255	...	3.9	1–0	...	0.150 ± 0.045[a]	575	8
	...	...	1–0	...	0.22 ± 0.05	575	9
	...	...	1–0	...	...	...	10
	...	3.9	2–1	...	∼0.81[b]	...	8
	...	3.9114	4–3	7.4 ± 1.0	3.7 ± 0.5	480 ± 35	11
	...	3.9115	4–3	7.3 ± 1.9	3.7 ± 0.4	500 ± 17[c]	12
	...	3.9118	4–3	7.5 ± 0.56	3.8 ± 0.4	...	12
	...	3.9113	6–5	14.3 ± 3.1	7.3 ± 0.7	500 ± 17[c]	12
	...	3.9109	9–8	17.9 ± 1.4	9.1 ± 0.8	...	11
	...	3.9111	9–8	21.9 ± 4.9	11.1 ± 2.2	500 ± 17[c]	12
	...	3.9119	9–8	24.2 ± 1.3	12.5 ± 2.4	...	12
	...	3.9101	10–9	23.3 ± 4.0	11.9 ± 2.4	500 ± 17[c]	12
	...	3.9110	11–10	20.5 ± 4.1	10.4 ± 2.1	500 ± 17[c]	12

Note.—For BR 1202-0725, N and S indicate the northern and southern components, respectively, and NS indicates an integrated measurement over both components.
[a] Derived for central ∼1″ only.
[b] Assuming a velocity-averaged brightness temperature ratio between ^{12}CO($J = 2 \rightarrow 1$) and ^{12}CO($J = 1 \rightarrow 0$) of 1.35 ± 0.55 (Papadopoulos et al. 2001).
[c] Derived from a line profile averaged over all transitions.

References.—(1) Carilli et al. 2002b; (2) Omont et al. 1996; (3) Ohta et al. 1996; (4) Carilli et al. 2002a; (5) Carilli et al. 2003; (6) Cox et al. 2002; (7) A. Weiss et al. 2006, in preparation; (8) Papadopoulos et al. 2001; (9) Lewis et al. 2002; (10) D. Riechers et al. 2006, in preparation; (11) Downes et al. 1999; (12) Weiss et al. 2006.

3.2. *PSS J2322+1944*

3.2.1. *Previous Results*

The $z = 4.12$ QSO PSS J2322+1944 is an IR-luminous high-redshift source (see Table 2) that is known to exhibit strong CO line emission in multiple transitions (see Table 3). Optical imaging and spectroscopy reveal a double-source structure, and the two components are separated by about 1.″5. The spectra of both peaks are essentially identical, consistent with strong gravitational lensing (optical magnification factor $\mu_L^{\rm opt} = 3.5$) by an intervening foreground galaxy (Carilli et al. 2003). In high-resolution VLA images, Carilli et al. (2003) find a molecular Einstein ring with a diameter of 1.″5 in ^{12}CO($J = 2 \rightarrow 1$) line emission, which can be modeled as a circumnuclear star-forming disk with a radius of 2.2 kpc (CO magnification factor $\mu_L^{\rm CO} \sim 2.5$). The derived intrinsic star formation rate (SFR) is of the order of 900 $M_\odot$ yr^{-1}. PSS J2322+1944 exhibits strong, nonthermal (synchrotron) radio continuum emission at 1.4 GHz, and the rest-frame radio-to-IR spectral energy distribution (SED) resembles that of local nuclear starburst galaxies such as M82 (Cox et al. 2002). This QSO is the fourth high-z CO emitter to be detected in [C I] emission (Pety et al. 2004), providing additional evidence for the presence of active star formation in the host galaxy.

3.2.2. *New Observations*

The final ^{12}CO($J = 1 \rightarrow 0$) spectra of PSS J2322+1944 are shown in Figure 2 (*top*, GBT; *middle*, Effelsberg; *bottom*, combined spectrum). From Gaussian fitting to the combined spectrum, the peak line flux density is found to be 0.77 ± 0.07 mJy, the line FWHM is 190 ± 14 km s^{-1}, and the integrated line flux is 0.155 ± 0.013 Jy km s^{-1}. These values are in good agreement with the ^{12}CO($J = 1 \rightarrow 0$) detection of Carilli et al. (2002a; $S_\nu = 0.89 \pm 0.22$ mJy, $\Delta V_{\rm FWHM} = 200 \pm 70$ km s^{-1}, $I = 0.19 \pm 0.08$ Jy km s^{-1}), although results for the higher J CO transitions indicate a larger line width ($\Delta V_{\rm FWHM} > 250$ km s^{-1}; see Table 3). The Gaussian fit gives a redshift of 4.1179 ± 0.0002. The derived lensing-corrected CO line luminosity of 4.2×10^{10} K km s^{-1} pc^2 results in an H_2 gas mass of 3.4×10^{10} $M_\odot$ (see also Table 2).

3.3. *APM 08279+5255*

3.3.1. *Previous Results*

APM 08279+5255 is a strongly lensed, radio-quiet broad absorption line (BAL) QSO at $z = 3.91$. Gravitational lens models of the QSO continuum source suggest magnification by a factor of $\mu_L^{\rm opt} \sim 100$, and the image breaks up into three components with a maximum separation of 0.″4 (Ledoux et al. 1998; Ibata et al. 1999; Egami et al. 2000). APM 08279+5255 has been detected in the millimeter and submillimeter dust continuum, revealing an apparent bolometric luminosity of $\sim 5 \times 10^{15}$ $L_\odot$ (Lewis et al. 1998). A multitransition CO study (see Table 3) in combination with detailed lens models appears to reveal a spatially extended structure on a scale of at least 400 pc (Lewis et al. 2002), which is gravitationally magnified by a factor of $\mu_L^{\rm CO} = 7$. The strength of the ^{12}CO($J = 9 \rightarrow 8$) emission indicates the presence of hot dense gas with a kinetic temperature of approximately 200 K (Downes et al. 1999).

From VLA imaging of the CO ground-state transition at a linear resolution of 2.″25, Papadopoulos et al. (2001) report the detection of an extended, low-excitation molecular gas reservoir around the compact nucleus that extends over a scale of 7″ (∼30 kpc). The integrated brightness temperature of this extended domain appears to be of the same order of magnitude as that of the nuclear region. This extended reservoir would be well within our 32″ GBT beam. Papadopoulos et al. (2001) do not derive the total flux in the extended reservoir. For the central ∼1″ (corresponding to ∼7.2 kpc at the source redshift), which they call "the nuclear ^{12}CO($J = 1 \rightarrow 0$) emission," they find an integrated flux of 0.150 ± 0.045 Jy km s^{-1}. The VLA bandpass used by Papadopoulos et al. (2001) has an effective bandwidth of ∼45 MHz, or ∼575 km s^{-1} at the ^{12}CO($J = 1 \rightarrow 0$) line frequency. Therefore, assuming that the peak in their Figure 1*c* is $6.5\sigma = 260$ μJy beam^{-1} ($\sigma = 40$ μJy beam^{-1}), we consistently derive an integrated flux over the peak of 0.15 Jy km s^{-1} beam^{-1}. However, Papadopoulos et al. (2001) suggest that this peak of "nuclear emission" sits on a broad, extended plateau (see their Fig. 1*c*). If we assume that the extended reservoir component is traced by their 2 σ (80 μJy beam^{-1}) contour, it has a width of $\sim 8'' \times 3''$, or ∼4.7 beam areas at the given resolution of 2.″25 × 2.″25. This corresponds to a flux of 0.22 Jy km s^{-1} for the extended emission. The same estimate for their 3 σ (120 μJy beam^{-1}) contour gives a width of $\sim 7'' \times 2.''25$, or ∼3.1 beam areas. This again corresponds to a flux of 0.22 Jy km s^{-1} (note that both these estimates are lower limits for the extended emission). The total flux in the ^{12}CO($J = 1 \rightarrow 0$) map of Papadopoulos et al. (2001) is therefore estimated to be $\gtrsim$0.37 Jy km s^{-1}. The same authors also suggest that this reservoir breaks up into multiple components at higher resolution; in their ^{12}CO($J = 2 \rightarrow 1$) observations at 0.″5 resolution, they claim to find two emitting regions 2″–3″ distant from the central region; if real, these could be companion galaxies that are not individually resolved in the extended ^{12}CO($J = 1 \rightarrow 0$) reservoir.

3.3.2. *New Observations*

The final ^{12}CO($J = 1 \rightarrow 0$) spectrum of APM 08279+5255 is shown in Figure 3. We derive a ^{12}CO($J = 1 \rightarrow 0$) peak flux of 0.26 ± 0.04 mJy and a FWHM of 556 ± 55 km s^{-1} from our Gaussian fit. This results in an integrated line flux of 0.152 ± 0.020 Jy km s^{-1}, which is in good agreement with the value of 0.150 ± 0.045 Jy km s^{-1} found by Papadopoulos et al. (2001) for the central ∼1″ ["the nuclear ^{12}CO($J = 1 \rightarrow 0$) emission"]. However, our result is inconsistent with the integrated flux of 0.37 Jy km s^{-1} given by our estimate of their full ^{12}CO($J = 1 \rightarrow 0$) reservoir (see previous subsection). Such a high flux is clearly ruled out by our GBT observations. We thus find no evidence for a luminous extended halo, which would be well within our 32″ beam, and cannot confirm the existence of bright companion galaxies. The derived FWHM velocity width of our ^{12}CO($J = 1 \rightarrow 0$) detection is in agreement with single-dish observations of the ^{12}CO($J = 6 \rightarrow 5$), ^{12}CO($J = 10 \rightarrow 9$), and ^{12}CO($J = 11 \rightarrow 10$) transitions obtained with the IRAM 30 m telescope (∼500 km s^{-1}; Weiss et al. 2006) and IRAM Plateau de Bure interferometer observations of the ^{12}CO($J = 4 \rightarrow 3$) transition (480 ± 35 km s^{-1}; Downes et al. 1999; see Table 3). Our derived ^{12}CO($J = 1 \rightarrow 0$) redshift of 3.9122 ± 0.0007 is in good agreement with previous results (3.9114 ± 0.0003 for the $4 \rightarrow 3$ transition). The derived lensing-corrected CO line luminosity of 1.4×10^{10} K km s^{-1} pc^2 results in an H_2 gas mass of 1.1×10^{10} $M_\odot$ (see also Table 2).

4. ANALYSIS AND DISCUSSION

4.1. *Large Velocity Gradient Modeling*

To investigate how much of the ^{12}CO($J = 1 \rightarrow 0$) emission in our target QSOs is associated with the molecular gas reservoirs detected in the higher J CO transitions, we have used spherical, one-component large velocity gradient (LVG) models. All these LVG calculations use the collision rates from Flower & Pineau des Forets

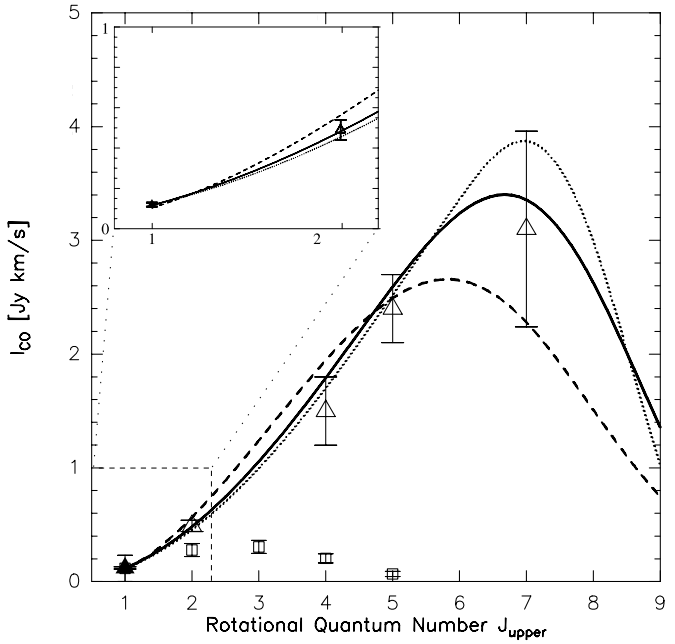

FIG. 4.—CO ladder and LVG models (based on all $J > 1$ transitions) for BR 1202−0725. The inset shows a zoomed-in version of the $J = 2$, 1 region (as indicated by the dashed box). The filled triangle is the ^{12}CO($J = 1 \rightarrow 0$) data point based on the combined spectrum. Data for the higher J CO transitions (*open triangles*) are taken from the literature (see Table 3). For comparison, we also show data for the inner disk of the Milky Way (*open squares*; Fixsen et al. 1999), normalized to the ^{12}CO($J = 1 \rightarrow 0$) flux of BR 1202−0725. The kinetic temperature T_{kin} and gas density $\rho_{gas}(H_2)$ are treated as free parameters in this study. Three representative models are shown: Model 1 (*solid line*) assumes $T_{kin} = 60$ K and $\rho_{gas}(H_2) = 10^{4.1}$ cm^{-3} and gives the overall best fit to all transitions. Model 2 (*dashed line*) assumes $T_{kin} = 120$ K and $\rho_{gas}(H_2) = 10^{3.7}$ cm^{-3}, while model 3 (*dotted line*) assumes $T_{kin} = 30$ K and $\rho_{gas}(H_2) = 10^{4.6}$ cm^{-3}.

(2001) with an ortho/para H_2 ratio of 3 and a CO abundance per velocity gradient of $[CO]/(dv/dr) = 1 \times 10^{-5}$ pc (km s^{-1})$^{-1}$ (e.g., Weiss et al. 2005). Models were fitted to those lines *above* the ^{12}CO($J = 1 \rightarrow 0$) transition listed in Table 3 for each source. The turnover of the CO line SED (and therefore the slope beyond the turnover) is not well determined. Thus, a large degeneracy exists between the kinetic gas temperature T_{kin} and density $\rho_{gas}(H_2)$, the two main free parameters in our study. As an example, Figure 4 shows data of all transitions and three representative models for BR 1202−0725: Model 1 (*solid line*) assumes $T_{kin} = 60$ K and $\rho_{gas}(H_2) = 10^{4.1}$ cm^{-3} and gives the overall best fit to all transitions. Models 2 (*dashed line*) and 3 (*dotted line*) are shown as a representation of the parameter space allowed by the data within the error bars. Model 2 assumes $T_{kin} = 120$ K and $\rho_{gas}(H_2) = 10^{3.7}$ cm^{-3}, while model 3 assumes $T_{kin} = 30$ K and $\rho_{gas}(H_2) = 10^{4.6}$ cm^{-3}. The LVG predicted ^{12}CO($J = 1 \rightarrow 0$) flux of the different models based on the $J > 1$ CO transitions is fairly well constrained by the solutions. Most of our calculated models suggest that the CO emission is close to thermalized up to the ^{12}CO($J = 4 \rightarrow 3$) transition and optically thick ($\tau \gtrsim 5$), which implies that the LVG predicted ^{12}CO($J = 1 \rightarrow 0$) line fluxes are similar to those we would derive by assuming a ν^2 scaling of the line flux densities from the mid-J CO transitions. The predicted LVG integrated flux ranges of the ^{12}CO($J = 1 \rightarrow 0$) transition are 0.10–0.12 Jy km s^{-1} (BR 1202−0725), 0.20–0.23 Jy km s^{-1} (PSS J2322+1944), and 0.13–0.20 Jy km s^{-1} (APM 08279+5255) and are in good agreement with our observations for all sources. As described in § 3.2.2, the observed ^{12}CO($J = 1 \rightarrow 0$) line width in our new observations and in the VLA spectrum (Carilli et al. 2002a) of PSS J2322+1944 is lower than that of the higher J transitions; thus, the integrated model fluxes are a bit higher than our result. If we compare the peak fluxes only, we obtain a good agreement.

Our observations and models are in agreement with the assertion that *all* observed ^{12}CO($J = 1 \rightarrow 0$) flux density is associated with the highly excited molecular gas seen in the high-J CO lines. We thus find no evidence for an additional luminous, more extended low surface brightness gas component surrounding the central region of our target QSOs, in contrast to what has been suggested previously for APM 08279+5255 (Papadopoulos et al. 2001). Given the accuracy of our measurements, we conclude that at most 20%–30% of the ^{12}CO($J = 1 \rightarrow 0$) luminosity may be associated with such a diffuse component. We note, however, that if the L'_{CO} to $M_{gas}(H_2)$ conversion factor (α) for a faint extended component were higher (e.g., Galactic), a higher H_2 mass may be hidden in such an extended component.

4.2. *Correlations of High- and Low-Redshift Galaxies*

CO results for our three high-redshift IR-luminous QSOs are summarized in Tables 1 and 2. Our sample consists of all three high-z QSOs for which the CO ground-state transition has been detected to date and covers ~20% of the CO-detected $z > 2$ quasars. As discussed above, the ^{12}CO($J = 1 \rightarrow 0$) transition provides the best information of the total amount of molecular gas in a system, quantified by $L'_{CO(1-0)}$. For most QSOs/galaxies detected in CO at high z, ^{12}CO($J = 3 \rightarrow 2$) and ^{12}CO($J = 4 \rightarrow 3$) are the lowest transitions that have been detected to date. Based on our results in the previous paragraph, however, we can now estimate their $L'_{CO(1-0)}$ by assuming constant brightness temperature for all transitions from ^{12}CO($J = 1 \rightarrow 0$) to ^{12}CO($J = 4 \rightarrow 3$) (i.e., L'_{CO} is the same for those transitions). This assumption is also in agreement with observations toward the radio galaxy 4C 60.07 (Greve et al. 2004). However, it is important to note that all high-z sources were selected via higher J CO transitions, which could, in principle, introduce a bias toward highly excited starburst environments.

Following Sanders et al. (1991), Gao & Solomon (2004) found a nonlinear relation between the logarithms of the FIR luminosity L_{FIR} and the ^{12}CO($J = 1 \rightarrow 0$) line luminosity L'_{CO} for a sample of local spiral galaxies, luminous infrared galaxies, and ultraluminous infrared galaxies. Their sample consists mostly of galaxies whose FIR luminosity is powered by star formation only. Our ^{12}CO($J = 1 \rightarrow 0$) observations and LVG models suggest that L'_{CO} can be estimated for all CO-detected high-z sources with some degree of confidence, even if only observations of higher J CO transitions exist for most of these sources. To put this result into context, we now aim to discuss the L'_{CO}–L_{FIR} relation and its implications for some selected samples of galaxies at low and high redshift.

Figure 5 shows the relationship between log L_{FIR} and log L'_{CO} for our three targets, all other high-z CO detections (except TN J0924−2201, which does not have a measured FIR luminosity), the $z < 0.2$ Palomar-Green (PG) QSOs from Alloin et al. (1992), Evans et al. (2001), and Scoville et al. (2003) including PDS 456 (Yun et al. 2004), local ($z < 0.3$) ULIRGs from Solomon et al. (1997), and the local galaxy sample ($z < 0.1$) of Gao & Solomon (2004). All FIR luminosities for the high-z sources are rederived as described by Carilli et al. (2005) unless stated otherwise. Lensing magnification factors were taken into account. In addition, data for the Milky Way disk (Fixsen et al. 1999) and an (extrapolated) relation for Galactic molecular clouds (Mooney & Solomon 1988) are given for comparison. The solid line is a straight-line least-squares fit to the Gao & Solomon (2004) sample, corresponding

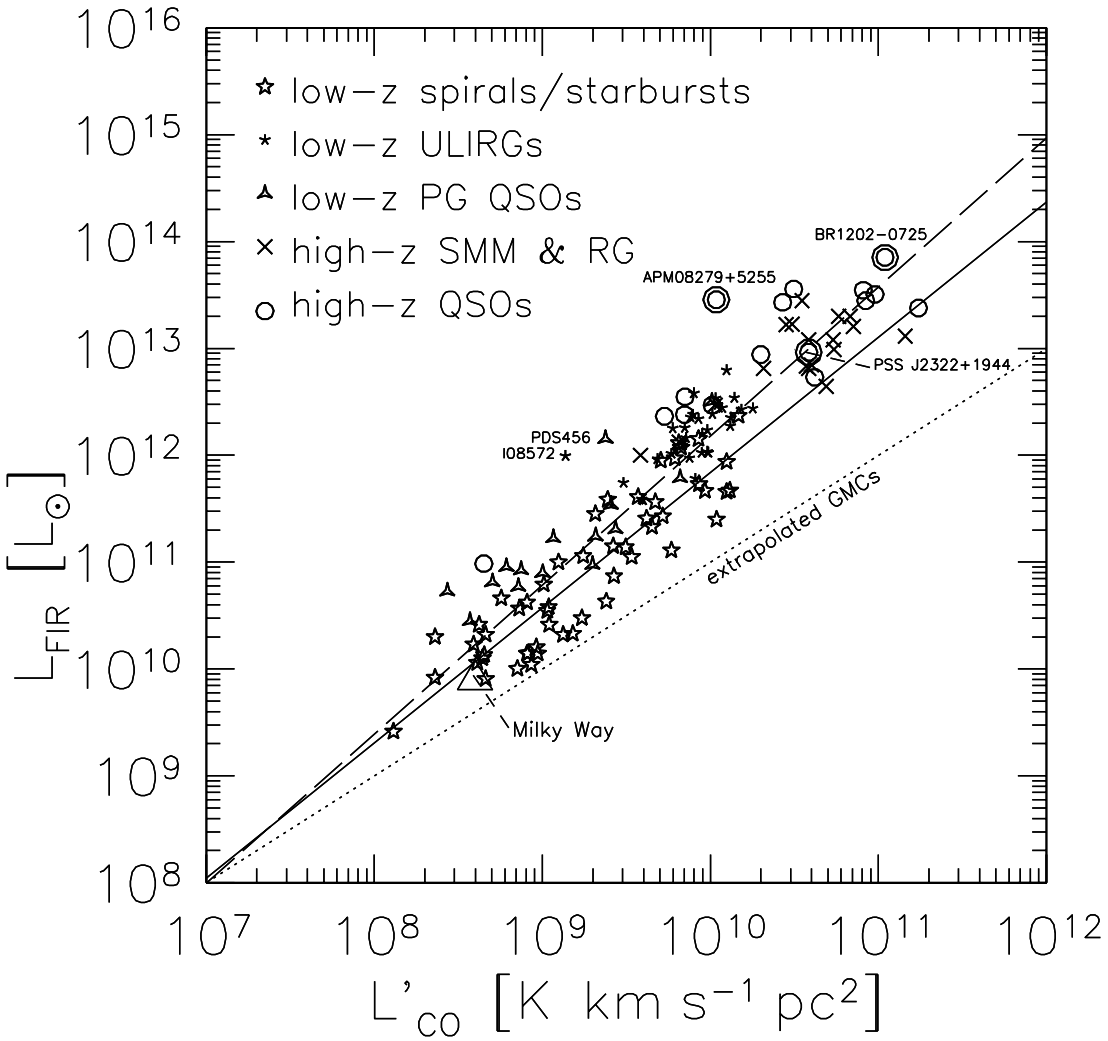

FIG. 5.—Comparison of velocity-integrated CO line luminosity with FIR luminosity for a sample of low-z spiral and starburst galaxies from Gao & Solomon (2004), the ULIRGs from Solomon et al. (1997), $z < 0.2$ PG QSOs from Alloin et al. (1992), Evans et al. (2001), and Scoville et al. (2003), extrapolated Galactic molecular clouds (GMCs) from Mooney & Solomon (1988), the Milky Way (Fixsen et al. 1999), and high-z submillimeter galaxies, radio galaxies, and QSOs from the literature (see Solomon & Vanden Bout 2005) with respect to our new results. All FIR luminosities are rederived as described in Carilli et al. (2005). All data are corrected for gravitational lensing. The solid line is a straight-line least-squares fit to the Gao & Solomon (2004) sample, corresponding to $\log L_{\rm FIR} = (1.26 \pm 0.08) \log L_{\rm CO} - 0.81$. The dotted line shows the fit to the GMCs from Mooney & Solomon (1988), corresponding to a power-law index of 0.96 ± 0.08. The dashed line is a fit to all high-z sources, the Gao & Solomon (2004) data, the Solomon et al. (1997) ULIRGs, and the PG QSOs, corresponding to $\log L_{\rm FIR} = (1.39 \pm 0.05) \log L_{\rm CO} - 1.76$.

to $\log L_{\rm FIR} = (1.26 \pm 0.08) \log L_{\rm CO} - 0.81$ (the power-law index is 1.25 ± 0.08 in the original publication). Fitting the high-z sources, the Gao & Solomon (2004) data, the Solomon et al. (1997) ULIRGs, and the PG QSOs together, we find the relation $\log L_{\rm FIR} = (1.39 \pm 0.05) \log L_{\rm CO} - 1.76$. Both relations are clearly nonlinear, as their power-law indexes are significantly larger than unity (see also the corresponding discussion in Gao & Solomon 2004). We recover a Schmidt-Kennicutt law (power-law index of 1.4; Kennicutt 1998a, 1998b) for the larger, more heterogeneous sample. More importantly, the high-z sources seem to follow the same slope (within the errors) as seen at low z, even though most high-z sources harbor central active galactic nuclei (AGNs). In addition, the high-z QSOs and high-z submillimeter and radio galaxies (likely lacking a luminous AGN) statistically occupy the same area in the plot. The same behavior is found for the PG QSOs in comparison to the low-z spiral galaxies, LIRGs, and ULIRGs. It is in general not clear that the FIR emission comes mostly from star formation, i.e., that it is not strongly biased by active nuclei or the interstellar radiation field. For example, SED modeling of the $z = 2.6$ quasar H1413+117 (the Cloverleaf) reveals that only $\sim$20% of its FIR luminosity is powered by star formation (Solomon et al. 2003), but it is not an outlier in the $L'_{\rm CO}$-$L_{\rm FIR}$ diagram. In this context, the elevated $L_{\rm FIR}/L'_{\rm CO}$ ratio in APM 08279+5255 may be explained by a combination of differential lensing and a relatively high contribution of the AGN to $L_{\rm FIR}$ (see Rowan-Robinson 2000 for models of the IR SED). Outliers such as APM 08279+5255 are also found at low z (e.g., the QSO PDS 456 and the warm ULIRG IRAS 08572+3915; see Fig. 5). As the relative number of such outliers is very small, this may also be explained by a brief FIR-bright AGN phase (Yun et al. 2004). However, it is likely that the dominant energy source in most ULIRGs is an extreme starburst rather than heating by a dust-enshrouded AGN (e.g., Solomon et al. 1997; Downes & Solomon 1998). This picture is supported by the finding that ULIRGs harbor large quantities of *dense* molecular gas, which is more intimately involved with star formation than the major fraction of the mostly diffuse CO (Gao & Solomon 2004). It has to be kept in mind that the high-z sources are highly selected and probably fulfill the Malmquist bias (i.e., the apparent increase in the average $L'_{\rm CO}$ and $L_{\rm FIR}$ toward high redshift is

probably a consequence of the flux limitation in the sample; e.g., Sandage 1994). As an additional consequence of flux limitation in the sample, lensing influences the results (i.e., stronger lensing magnification allows us to probe deeper, and therefore the intrinsic CO luminosity drops).

We can also set an approximate lower limit on the duration of the intense starburst phase. Considering the total H_2 masses and star formation rates in Table 2, the depletion timescale of the molecular gas is of the order of 10^7 yr for all three QSOs under the assumption of a constant SFR and 100% star-forming efficiency. This implies that the starburst itself can be relatively short-lived (and compact, as the dynamical time must be less than the starburst lifetime), unless the molecular gas in which the star formation occurs can be resupplied on timescales of $\sim 10^7$ yr.

5. SUMMARY

We have detected ^{12}CO($J = 1 \rightarrow 0$) emission in three QSOs at redshifts $3.9 < z < 4.7$ with the NRAO GBT and the MPIfR Effelsberg telescope. From our analysis of the resulting spectra of BR 1202−0725, PSS 2322+1944, and APM 08279+5255, we obtain the following results:

1. We derived lensing-corrected ^{12}CO($J = 1 \rightarrow 0$) line luminosities of 1.0×10^{11} K km s^{-1} pc^2 for BR 1202−0725, 4.2×10^{10} K km s^{-1} pc^2 for PSS 2322+1944, and 1.4×10^{10} K km s^{-1} pc^2 for APM 08279+5255. These results are in good agreement (within a factor of 2) with previous estimates of the total CO luminosities based on the higher J CO transitions, consistently providing very large $M_{\rm gas}(H_2)$ of $>10^{10}\ M_\odot$.

2. ^{12}CO($J = 1 \rightarrow 0$) fluxes predicted by one-component LVG models are in good agreement with our observations. Considering our modeling results, the CO emission appears to be close to thermalized up to the $4 \rightarrow 3$ transition in all cases. Thus, our observations show no indication of a luminous extended, low surface brightness molecular gas component in any of the high-redshift QSOs in our sample (cf. Papadopoulos et al. 2001). In fact, all CO transitions are described very well by a single gas component in which all molecular gas is concentrated in a compact circumnuclear region. If such extended components were to exist, our observations and models would limit their contribution to the overall luminosity to at most 20%–30%.

3. There appears to be a correlation between $\log L_{\rm FIR}$ and $\log L'_{\rm CO}$ for low-redshift galaxies including (U)LIRGs over orders of magnitude in $L_{\rm FIR}$, and the significantly brighter sources found at high z appear to follow the same general trend (see also Solomon & Vanden Bout 2005). In particular, we find that the correlation shows no significant difference between QSOs and systems without a luminous AGN.

The observations presented herein demonstrate the feasibility of detecting high-z CO with 100 m single-dish radio telescopes and highlight the physical implications of observing the ground-state transition of this molecule toward massive galaxies at redshifts greater than 4.

The National Radio Astronomy Observatory is operated by Associated Universities, Inc., under cooperative agreement with the National Science Foundation. We would like to thank the staff at the GBT, in particular J. Braatz, G. I. Langston, and R. J. Maddalena, for their extensive support and many helpful discussions. D. R. acknowledges support from Deutsche Forschungsgemeinschaft (DFG) Priority Programme 1177. C. C. acknowledges support from the Max-Planck-Gesellschaft and the Alexander von Humboldt-Stiftung through the Max-Planck-Forschungspreis. We thank the referee for many useful comments that helped to improve the manuscript.

REFERENCES

Alloin, D., Barvainis, R., Gordon, M. A., & Antonucci, R. R. J. 1992, A&A, 265, 429
Beelen, A., Cox, P., Benford, D. J., Dowell, C. D., Kovács, A., Bertoldi, F., Omont, A., & Carilli, C. L. 2006, ApJ, 642, 694
Bertoldi, F., et al. 2003, A&A, 409, L47
Carilli, C. L., Lewis, G. F., Djorgovski, S. G., Mahabal, A., Cox, P., Bertoldi, F., & Omont, A. 2003, Science, 300, 773
Carilli, C. L., et al. 2002a, ApJ, 575, 145
———. 2002b, AJ, 123, 1838
———. 2005, ApJ, 618, 586
Cox, P., et al. 2002, A&A, 387, 406
Downes, D., Neri, R., Wiklind, T., Wilner, D. J., & Shaver, P. A. 1999, ApJ, 513, L1
Downes, D., & Solomon, P. M. 1998, ApJ, 507, 615
Egami, E., Neugebauer, G., Soifer, B. T., Matthews, K., Ressler, M., Becklin, E. E., Murphy, T. W., Jr., & Dale, D. A. 2000, ApJ, 535, 561
Evans, A. S., Frayer, D. T., Surace, J. A., & Sanders, D. B. 2001, AJ, 121, 1893
Fan, X., et al. 2001, AJ, 122, 2833
Fixsen, D. J., Bennett, C. L., & Mather, J. C. 1999, ApJ, 526, 207
Flower, D. R., & Pineau des Forets, G. 2001, MNRAS, 323, 672
Gao, Y., & Solomon, P. M. 2004, ApJ, 606, 271
Greve, T. R., Ivison, R. J., & Papadopoulos, P. P. 2004, A&A, 419, 99
Guilloteau, S., Omont, A., Cox, P., McMahon, R. G., & Petitjean, P. 1999, A&A, 349, 363
Hu, E. M., Cowie, L. L., McMahon, R. G., Capak, P., Iwamuro, F., Kneib, J.-P., Maihara, T., & Motohara, K. 2002, ApJ, 568, L75
Hu, E. M., McMahon, R. G., & Egami, E. 1996, ApJ, 459, L53
Ibata, R. A., Lewis, G. F., Irwin, M. J., Lehár, J., & Totten, E. J. 1999, AJ, 118, 1922
Kennicutt, R. C., Jr. 1998a, ApJ, 498, 541
———. 1998b, ARA&A, 36, 189
Klamer, I. J., Ekers, R. D., Sadler, E. M., & Hunstead, R. W. 2004, ApJ, 612, L97
Klamer, I. J., Ekers, R. D., Sadler, E. M., Weiss, A., Hunstead, R. W., & De Breuck, C. 2005, ApJ, 621, L1
Kodaira, K., et al. 2003, PASJ, 55, L17
Ledoux, C., Theodore, B., Petitjean, P., Bremer, M. N., Lewis, G. F., Ibata, R. A., Irwin, M. J., & Totten, E. J. 1998, A&A, 339, L77
Lewis, G. F., Carilli, C., Papadopoulos, P., & Ivison, R. J. 2002, MNRAS, 330, L15
Lewis, G. F., Chapman, S. C., Ibata, R. A., Irwin, M. J., & Totten, E. J. 1998, ApJ, 505, L1
Mooney, T. J., & Solomon, P. M. 1988, ApJ, 334, L51
Ohta, K., Yamada, T., Nakanishi, K., Kohno, K., Akiyama, M., & Kawabe, R. 1996, Nature, 382, 426
Omont, A., Cox, P., Bertoldi, F., McMahon, R. G., Carilli, C., & Isaak, K. G. 2001, A&A, 374, 371
Omont, A., Petitjean, P., Guilloteau, S., McMahon, R. G., Solomon, P. M., & Pecontal, E. 1996, Nature, 382, 428
Ott, M., Witzel, A., Quirrenbach, A., Krichbaum, T. P., Standke, K. J., Schalinski, C. J., & Hummel, C. A. 1994, A&A, 284, 331
Papadopoulos, P., Ivison, R., Carilli, C. L., & Lewis, G. 2001, Nature, 409, 58
Pety, J., Beelen, A., Cox, P., Downes, D., Omont, A., Bertoldi, F., & Carilli, C. L. 2004, A&A, 428, L21
Rhoads, J. E., & Malhotra, S. 2001, ApJ, 563, L5
Rowan-Robinson, M. 2000, MNRAS, 316, 885
Sandage, A. 1994, ApJ, 430, 1
Sanders, D. B., Scoville, N. Z., & Soifer, B. T. 1991, ApJ, 370, 158
Scoville, N. Z., Frayer, D. T., Schinnerer, E., & Christopher, M. 2003, ApJ, 585, L105
Solomon, P. M., Downes, D., Radford, S. J. E., & Barrett, J. W. 1997, ApJ, 478, 144
Solomon, P. M., Radford, S. J. E., & Downes, D. 1992, Nature, 356, 318
Solomon, P. M., & Vanden Bout, P. A. 2005, ARA&A, 43, 677
Solomon, P. M., Vanden Bout, P. A., Carilli, C. L., & Guelin, M. 2003, Nature, 426, 636
Spergel, D. N., et al. 2003, ApJS, 148, 175
Taniguchi, Y., et al. 2005, PASJ, 57, 165
Vanden Bout, P. A., Solomon, P. M., & Maddalena, R. J. 2004, ApJ, 614, L97

Walter, F., Carilli, C., Bertoldi, F., Menten, K., Cox, P., Lo, K. Y., Fan, X., & Strauss, M. A. 2004, ApJ, 615, L17
Walter, F., et al. 2003, Nature, 424, 406
Weiss, A., Downes, D., Neri, R., Walter, F., Henkel, C., Wilner, D. J., Wagg, J., & Wiklind, T. 2006, A&A, submitted
Weiss, A., Neininger, N., Hüttemeister, S., & Klein, U. 2001, A&A, 365, 571
Weiss, A., Walter, F., & Scoville, N. Z. 2005, A&A, 438, 533
Yun, M. S., Carilli, C. L., Kawabe, R., Tutui, Y., Kohno, K., & Ohta, K. 2000, ApJ, 528, 171
Yun, M. S., Reddy, N. A., Scoville, N. Z., Frayer, D. T., Robson, E. I., & Tilanus, R. P. J. 2004, ApJ, 601, 723